Journal of Energy Storage 24 (2019) 100758

Contents lists available at ScienceDirect

Journal of Energy Storage

journal homepage: www.elsevier.com/locate/est

A hybrid model predictive and fuzzy logic based control method for state of power estimation of series-connected Lithium-ion batteries in HEVs

M.J. Esfandyari[a,b], M.R. Hairi Yazdi[a,*], V. Esfahanian[a,b], M. Masih-Tehrani[c], H. Nehzati[a,b], O. Shekoofa[d]

[a] School of Mechanical Engineering, University of Tehran, Tehran, Iran
[b] Vehicle, Fuel and Environment Research Institute (VFERI), University of Tehran, Tehran, Iran
[c] School of Automotive Engineering, Iran University of Science and Technology, Tehran, Iran
[d] Sattelite Research Institute, Iranian Space Research Center, Tehran, Iran

ARTICLE INFO

Keywords:
State of power estimation
Hybrid model predictive and fuzzy control
Cell-to-cell variation
Battery aging state

ABSTRACT

Accurate estimation of the State of Power (SoP) can ensure safe and efficient operation of Lithium-ion batteries in Electric Vehicles (EVs) and Hybrid Electric Vehicles (HEVs). The cell-to-cell variation within a battery pack is a major challenge towards accurate estimation of the SoP, particularly when the cells get aged. This paper presents a hybrid model predictive and fuzzy logic based control system to accurately estimate the SoP for series-connected Lithium-ion cells. The estimation strategy consists of two steps; the power capability for a single new cell is first reckoned under the light of the model predictive control algorithm. The second step is devoted to designation of a model-less fuzzy logic based control system to compensate for the concurrent aging state and State of Charge (SoC) differences among the cells. Accordingly, the present approach only utilizes the actual values of current and cell voltages together with the Electric Circuit Model (ECM) parameters of the new cell, which are identified off-line. Moreover, it benefits from a closed-loop framework which ends in an accurate and reliable SoP estimation. An experimental setup consisting of fresh and aged $LiFePO_4$ cell samples is designed and the extracted data are utilized to verify the proposed estimation method in a feed-forward simulation model for a HEV. The results indicate that the proposed method can estimate the pack SoP accurately while the safe operation for the cells is guaranteed.

1. Introduction

Today, the Lithium-Ion Batteries (LIBs) are increasingly used as the energy storage system in Electric Vehicles (EVs) and Hybrid Electric Vehicles (HEVs) [1–3]. The LIBs are very sensitive to the operational and environmental conditions such that their life cycle will be greatly reduced due to abuse [4–6]. The guaranteed safe operation of the battery in electric vehicles is achieved using the Battery Management System (BMS) which is responsible for monitoring and protection of the battery against misuse [7–9]. One of the most important tasks of the BMS is to estimate the battery maximum available power, also called the *State of Power (SoP)*. The battery SoP is defined as the maximum power which can be drawn from or received by the battery for some future seconds such that its Safe Operating Area (SOA) is not violated. This battery state is used in the Vehicle Control Unit (VCU) to enhance the performance while maintaining the safe operation of batteries in electric vehicles [10–12]. Battery power capability is limited by the allowable ranges of current, voltage, temperature and SoC which approve the safe operation of the battery. However, for a short prediction horizon (less than 10 s) mostly the current and voltage act as the limiting factors of the battery power capability and the temperature and SoC play a secondary role due the their slow changes.

Among the available techniques for estimation of battery SoP, methods based on battery Electric Circuit Model (ECM) are the most promising approaches due to consideration of battery dynamic behavior [13–15]. The existing researches for SoP estimation mainly differ in the applied ECM for the battery. It is clear that more precise ECMs paves the way through more accurate SoP estimations [14,16,17]. Simulating the electrochemical phenomena inside the battery, various ECMs and corresponding SoP estimations have been presented. This includes considering the polarization effect [18] and the dependence of polarization resistance to battery SoC [19,20], current [21–23], or both [24]. The change of battery ECM parameters as a result of aging is also an important issue which should be taken into account in the SoP

* Corresponding author.
E-mail address: myazdi@ut.ac.ir (M.R. Hairi Yazdi).

https://doi.org/10.1016/j.est.2019.100758
Received 11 February 2019; Received in revised form 30 April 2019; Accepted 1 May 2019

Nomenclature

EV	Electric vehicle
HEV	Hybrid electric vehicle
SoP	State of power
SoC	State of charge
SoH	State of health
ECM	Electric circuit model
LIB	Lithium-ion battery
BMS	Battery management system
VCU	Vehicle control unit
GPC	Generalized predictive control
MPC	Model predictive control
CAN	Controller area network
DC	Direct current
USB	Universal serial bus
PC	Personal computer
QP	Quadratic programming
SOA	Safe operating area
FLBC	Fuzzy logic based controller
RE	Relative error
i_s^{dis}	Secondary current limit at discharge
i_s^{chg}	Secondary current limit at charge
v_s^{dis}	Secondary voltage limit at discharge
v_s^{chg}	Secondary voltage limit at charge
K_e	Input scaling factor
K_u	Output scaling factor
V_{oc}	Open circuit voltage
R_i	Series resistance
C_{dl}	Double-layer capacitance
R_{ct}	Charge transfer resistance
ΔT	Prediction time window
V_c	RC branch voltage
V_t	Terminal voltage
k	Discrete time
T_s	Discretization sampling time
z, Z	Normalized SoC, element and vector
Q	Capacity
η	Coulombic efficiency
i, I	Current, element and vector
u,U	Input variable, element and vector
Y, Y_{ref}	Output and reference output vectors
Δu, ΔU	Input variable change, element and vector
Δi, ΔI	Current change, element and vector
N_p	Prediction horizon
N_c	Control horizon
i_{min}	Allowable charge current
i_{max}	Allowable discharge current
v_{min}	Cell voltage lower limit
v_{max}	Cell voltage upper limit
γ	Weighting factor
N_s	Number of series connected cells

estimation. The parameters of the model should be updated on-line in order to adapt the estimation with various aging levels [25–27]. A new method for compensating the noise effect in SoP estimation is also proposed by Wei et al. in which the model is identified online using a so-called AF-RTLS[1] method [28].

Recently, the predictive control methods have been shown to be appealing for battery control problem [29–31]. In this regard, Xavier et al. applied the Model Predictive Control (MPC) algorithm to the problem of fast charging of LIB [32,33]. They used a modified form of the MPC algorithm to compute a fast charging profile respecting the operating constraints of the battery. Also, Liu et al. used the constrained Generalized Predictive Control (GPC) algorithm for the fast charge problem where the ECM is coupled with the thermal model of the battery [34]. In all of the above mentioned research, the battery SoP is estimated for a single cell. However, the battery system in electric vehicles consists of tens to hundreds of cells which are connected in series. Due to manufacturing tolerances and various operating conditions, the cells do not have the same dynamic behavior and this cell-to-cell variation will also be intensified as the battery getting aged [35]. This leads to different states of power for the cells which limit the power capability of the battery pack. A straightforward solution for SoP estimation of a battery pack is to estimate the SoP for each individual cell. Therefore, the ECM parameters for each individual cell should be estimated on-line. This way, the cell with the lowest magnitude of SoP limits the power capability of the pack. Considering the large number of series-connected cells in electric vehicle applications, this solution requires a high computing power.

Among many existing researches, few studies have focused on the SoP estimation for a battery pack considering cell-to-cell variation. Jin et al. proposed to use only the pack resistance, minimum/maximum values of the open circuit voltage for the cells and maximum resistance of the cells for estimating the pack SoP [36]. However, the estimation is performed conservatively for the worst case in which n folds of the SoP for an assumed cell with the maximum resistance and maximum or minimum open circuit voltage (depending whether the charge or the discharge power is estimated) is considered as the SoP of the pack, where n denotes the number of cells connected in series. Moreover, the effect of various aging states for the cells has not been taken into account for pack SoP estimation. Also, Dong et al. considered the differences in SoCs of the cells for battery pack SoP estimation in which an EKF-based method is used for estimating SoCs of the cells [37]. As a main drawback, they did not consider the change in SoP as the battery getting aged.

Waag et al. proposed a method for estimation of a LIB pack available power in which the weakest cell candidates are chosen according to the open circuit voltage and internal resistance values of the cells [23]. The estimated average cell parameters are then used to calculate the battery pack SoP. However, the dynamic of all the cells in the pack is assumed to be the same which is not necessarily correct in reality. Also, variation of the aging states for each individual cell has been considered using a simplified relation between the change in cell voltage and the change in pack average voltage. Jiang et al. proposed a novel ECM parameter estimation method and combined it with the mean cell model to estimate battery pack SoP [38]. Due to on-line estimation of ECM parameters for all the cells, the proposed method is adaptive to various aging states. But, the cell-to-cell variation caused by different SoCs of the cells and their effect on the pack SoP estimation are neglected. Also, a verification test to show the accuracy of battery pack SoP estimation is ignored.

In fact, the SoP variations among the cells are mainly caused by different SoCs and aging states of the cells and therefore, it seems necessary to consider both in order to obtain accurate estimations of the SoP for the battery pack. This has been remained as a major challenge towards accurate estimation of battery pack power capability. This is due to the fact that on-line estimation of ECM parameters for the cells considering the effect of both SoC and aging state variations not only increases the complexity and computational cost of battery SoP estimation, but also requires adequate lab and field validations to prove the accuracy and convergence of the on-line estimation algorithms [35,39].

[1] Adaptive Forgetting Recursive Total Least Squares

In this paper, a SoP estimation method for series-connected Lithium-ion cells is presented in which the SoC and aging state variations of the cells are taken into account simultaneously. First, the MPC algorithm is applied to accurately predict the power capability of a new cell. In this regard, the cell-based SoP estimations are compared with those presented by Sun et al. [27] and the results demonstrate that using MPC algorithm, the accuracy of SoP estimation is improved. In the second step, a model-less fuzzy logic based control system is designed to compensate for the cell-to-cell variation through a closed-loop interaction with the VCU. The closed-loop framework of the present technique paves the way through accurate and reliable SoP estimation for series-connected cells. In order to verify the pack-level estimations, the extracted data from an experimental setup for sample new and aged $LiFePO_4$ cells are utilized in a feed-forward simulation model for a series HEV. The driving cycle results indicate promising SoP estimations along with guaranteed safe operation for the battery pack.

Three major contributions of the paper are highlighted as follows: (1) Different dynamic behaviors of all the cells caused by various SoCs and aging states are taken into account for accurate estimation of the pack SoP; (2) Unlike the aforementioned researches which require online estimation of the ECM parameters for the cells, in the proposed method, no *a priori* aging state estimation of the cells is required and only the ECM parameters of the new cell are utilized which are identified off-line. Also, the SoP estimations are robust to inaccuracies in SoC values. (3) As a common method, the power capability is estimated assuming a constant-current reference case which leads to the cell voltage reaching its allowable limit at the end of the prediction time window. In the present study, this traditional estimation method is replaced by the well-known MPC algorithm which ends in more accurate SoP estimates, as verified by the results. Rest of the paper is organized as follows. In Section 2, the ECM for the cell is developed using an experimental setup. Then, the SoP estimation for the new cell based on the MPC algorithm is presented in Section 3. Considering the cell-to-cell variation, SoP estimation for a battery pack is addressed in Section 4. Finally, the verification results are presented in Section 5.

2. Battery model

As a preliminary step for SoP estimation of series-connected cells, an ECM for the cell is developed using an experimental setup where the details are explained in the following sections.

2.1. Equivalent circuit model structure

Components of the ECM of the battery, as presented in Fig. 1, consist of the open circuit voltage (V_{oc}), internal resistance (R_i) and one RC circuit which contains the double-layer capacitance (C_{dl}) and charge transfer resistance (R_{ct}). The dynamic equation for this model in discrete time is given by Eq. (1) [40,41].

$$\begin{cases} V_c(k+1) = V_c(k)e^{-\frac{\Delta T}{R_{ct}C_{dl}}} + R_{ct}(1 - e^{-\frac{\Delta T}{R_{ct}C_{dl}}})i(k+1) \\ V_t(k+1) = V_{oc}(k+1) - R_i i(k+1) - V_c(k+1) \end{cases} \quad (1)$$

where k indicates the sampling time, ΔT is the sampling interval, V_c is the RC circuit voltage, V_t is the terminal voltage and i is the battery current. To obtain the ECM parameters, experimental tests have been carried out which are described in the following section.

2.2. Battery experiments

The battery impedance parameters, the open circuit voltage and capacity for $LiFePO_4$ cell sample are obtained using an experimental setup. The major components of test bench, as illustrated in Fig. 2, consist of AVL DC power supply, $LiFePO_4$ cell, BMS, thermal chamber, CAN to USB interface, and host computer for data monitoring and command to the power supply. The AVL DC power supply can be used for charging and discharging of the batteries for currents up to ± 300 A. The cell voltages are read by the BMS with errors less than 0.1% (i.e. 5 mV in 0–5 volts range). Also, a shunt resistor of 12 mΩ is used for battery current measurement which gives errors less than 2%. The cell voltages and current values are sent to a high speed CAN bus by the BMS. In the host PC, a data monitoring and storage software is designed in LabVIEW environment which receives the CAN bus data using CANusb interface from Softing company [42]. The battery cell used in this research is $LiFePO_4$ cell with nominal capacity of 10 Ah and nominal voltage of 3.2 V.

In order to obtain capacity of the cell sample, the following test procedure is used [7,40]:

Charging with constant current rate of 0.5C until the battery terminal voltage reaches its maximum value of 3.65 V.

- The voltage is remained constant at 3.65 V until the current drops below 0.02C.
- After a rest period of 20 min, the battery is discharged with the constant current rate of 0.5C until the cut-off voltage of 2 V is reached.
- The total Ampere-hour passed from the battery during the discharge cycle indicates the battery capacity.

Following the above procedure, the new cell capacity is obtained to be 10.58 Ah. The identification of the battery ECM parameters is performed off-line using current pulses at different SoCs for each of the charge and discharge cases [43,44]. In this regard, starting from the fully charged state, the battery is discharged for 12 min with a current pulse of 0.5C rate. After a consequent rest of 20 min, the procedure is repeated for ten times. The same test procedure is performed for the charge case after the end of the discharge test, i.e. the battery is charged with ten sequences of charge pulses with subsequent rests. Fig. 3 shows the terminal voltage response of the cell during the discharge and charge pulse tests. As shown in a magnified view in Fig. 3, the rapid change in the terminal voltage between points A and B indicates the effect of the series resistance on the response (i.e. $R_i i$). Also, the gradual change of the terminal voltage reflects the charge-transfer phenomena and the response can be used for obtaining the charge-transfer resistance R_{ct} and double-layer capacitance C_{dl}. To do so, from Eq. (1) the battery terminal voltage between point B and point C can be written in the form given by Eq. (2).

$$V_t(k) = V_B + c_1(1 - e^{-c_2 k T_s});\ 0 \le k \le N \quad (2)$$

where T_s is the data sampling time and N indicates the total data samples during the interval [t_B-t_C]. Using MATLAB identification toolbox, values of c_1 and c_2 are identified for each pulse response. Accordingly, the ECM parameters are obtained using Eq. (3). The corresponding values of V_{oc}, R_i, R_{ct} and C_{dl} for the new cell at 25 °C are presented in Fig. 4.

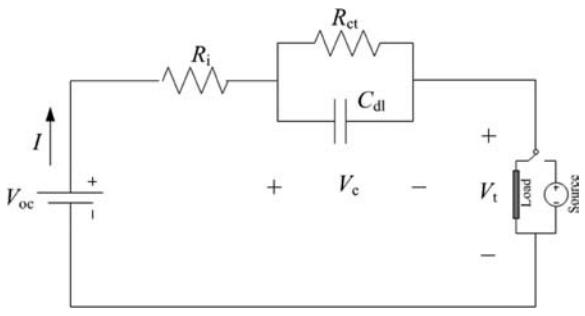

Fig. 1. Equivalent circuit model of the battery.

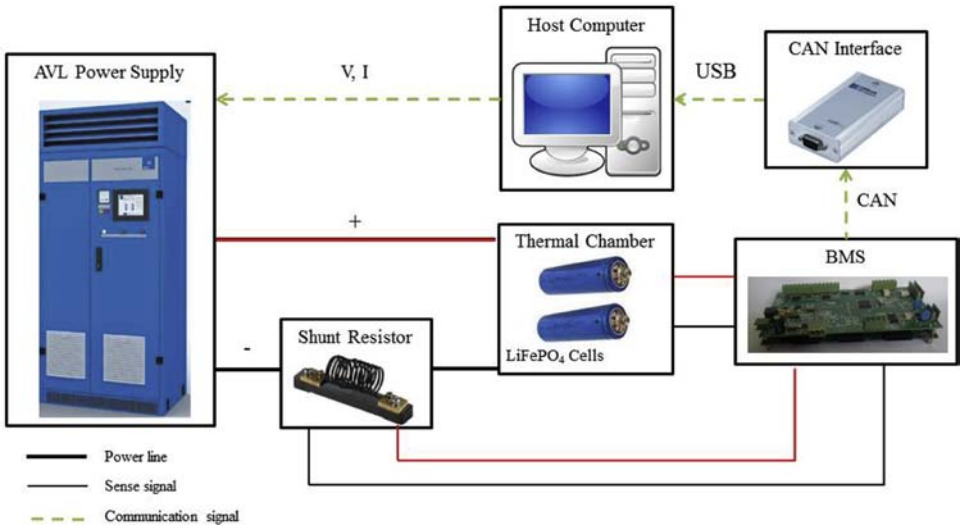

Fig. 2. The experimental setup.

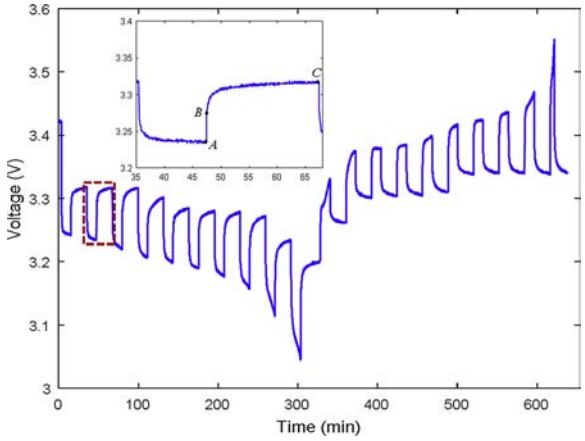

Fig. 3. Pulse test results for the new cell.

$$R_i = \frac{V_B - V_A}{i},\ R_{ct} = \frac{c_1}{i},\ C_{dl} = \frac{1}{c_2 R_{ct}} \tag{3}$$

3. MPC-based SoP estimation for the new cell

To obtain the SoP for series-connected cells, firstly the estimation is performed for a new cell based on the MPC algorithm. MPC relates to a class of control strategies that make use of predicted response of the system to optimize its future behavior while respecting the operating constraints. At each sample time, an optimal control sequence is calculated taking into account the future references of the controlled system where only the first control input is applied to the system [45,46]. In order to implement the MPC algorithm for estimation of battery SoP, the battery ECM should be transformed to a state space form which is compatible with the standard MPC algorithm. Then, an appropriate cost function reflecting the control objective should be defined and an on-line optimization problem considering the operating constraints on the inputs and outputs should be solved. The following sections provide the details for each of the aforementioned steps. The derived equations in this section are similar to what presented by Xavier et al. [32,33,47] for cell-level control of LIBs.

3.1. Battery state space representation

The ratio between the residual capacity and the total capacity of the battery indicates the SoC for the battery. Therefore, the SoC in discrete time can be represented by Eq. (4).

$$z(k+1) = z(k) - \frac{\eta \Delta t}{Q} i(k) \tag{4}$$

where $z(k)$ indicates the battery SoC (normalized to the interval [0,1]) at time sample k, η is the coulombic efficiency, ΔT is the time step, Q is the battery total capacity and $i(k)$ is the battery current which is assumed to be positive during the discharge. Considering the definition of battery SoC, the discrete time ECM model described by Eq. (1) can be written in state space form as given by Eqs. (5) and (6).

$$\begin{cases} x(k+1) = Ax(k) + Bu(k) \\ y(k) = Cx(k) + Du(k) \end{cases} \tag{5}$$

$$\begin{bmatrix} z(k+1) \\ v_c(k+1) \end{bmatrix} = \begin{bmatrix} 1 & 0 \\ 0 & e^{-\frac{\Delta T}{R_{ct}C_{dl}}} \end{bmatrix} \begin{bmatrix} z(k) \\ v_c(k) \end{bmatrix} + \begin{bmatrix} -\frac{\eta \Delta T}{Q} \\ R_{ct}(1 - e^{-\frac{\Delta T}{R_{ct}C_{dl}}}) \end{bmatrix} i(k)$$
$$V_t(k) - V_{oc}(z(k)) = [0 \ \ -1] \begin{bmatrix} z(k) \\ v_c(k) \end{bmatrix} + [-R_i] i(k) \tag{6}$$

In order to be compatible with the standard MPC formulation, the state space Eq. (5) should be written in the form given by Eq. (7) in which the direct feedthrough D-term is assumed to be zero and the system input is Δu rather than u.

$$\begin{aligned} x(k+1) &= Ax(k) + B\Delta u(k) \\ y(k) &= Cx(k) \end{aligned} \tag{7}$$

Defining a new state vector as $\tilde{x} = [x^T \ \ u^T]^T$, the state space Eq. (6) can be reformulated so that the feedthrough D-term is incorporated and the augmented model has an embedded integrator as represented by Eq. (8) [32,48].

$$\underbrace{\begin{bmatrix} x(k+1) \\ u(k+1) \end{bmatrix}}_{\tilde{x}(k+1)} = \underbrace{\begin{bmatrix} A & B \\ 0 & I \end{bmatrix}}_{\tilde{A}} \underbrace{\begin{bmatrix} x(k) \\ u(k) \end{bmatrix}}_{\tilde{x}(k)} + \underbrace{\begin{bmatrix} 0 \\ I \end{bmatrix}}_{\tilde{B}} \Delta u(k)$$
$$\tilde{y}(k) = \underbrace{[C \ \ D]}_{\tilde{C}} \underbrace{\begin{bmatrix} x(k) \\ u(k) \end{bmatrix}}_{\tilde{x}(k)} \tag{8}$$

where $\Delta u(k) = u(k+1) - u(k)$. Therefore, the state space Eq. (6) can be written in the following form:

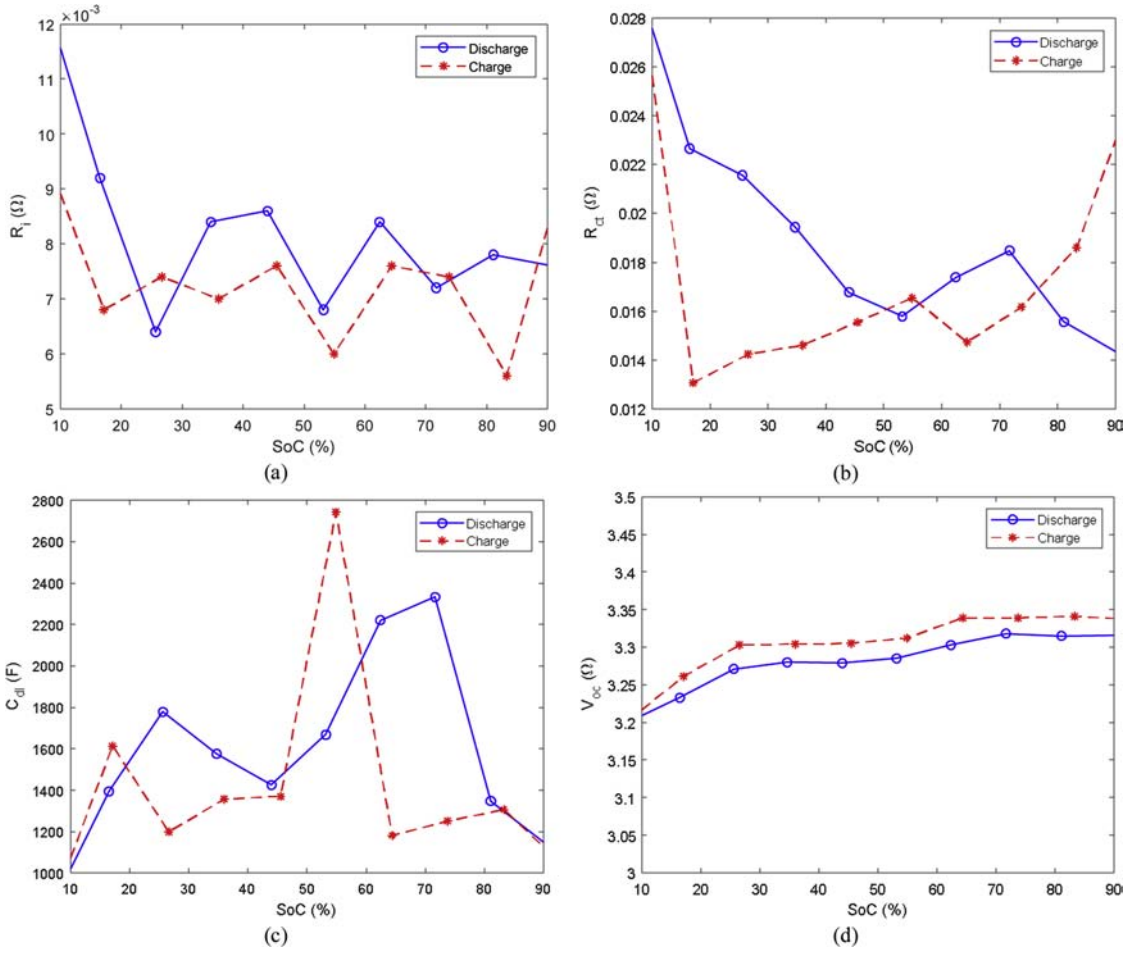

Fig. 4. ECM parameters for the new cell at 25 °C, (a) R_i, (b) R_{ct}, (c) C_{dl}, (d) V_{oc}.

$$\underbrace{\begin{bmatrix} z(k+1) \\ v_c(k+1) \\ i(k+1) \end{bmatrix}}_{\tilde{x}(k+1)} = \underbrace{\begin{bmatrix} 1 & 0 & -\frac{\eta \Delta T}{Q} \\ 0 & e^{-\frac{\Delta T}{R_{ct}C_{dl}}} & R_{ct}(1-e^{-\frac{\Delta T}{R_{ct}C_{dl}}}) \\ 0 & 0 & 1 \end{bmatrix}}_{\tilde{A}} \underbrace{\begin{bmatrix} z(k) \\ v_c(k) \\ i(k) \end{bmatrix}}_{\tilde{x}(k)} + \underbrace{\begin{bmatrix} 0 \\ 0 \\ 1 \end{bmatrix}}_{\tilde{B}} \underbrace{\Delta i(k)}_{\Delta u(k)}$$

$$\underbrace{V_t(k) - V_{oc}(z(k))}_{\tilde{y}_v(k)} = \underbrace{[0 \quad -1 \quad -R_i]}_{\tilde{C}_v} \underbrace{\begin{bmatrix} z(k) \\ v_c(k) \\ i(k) \end{bmatrix}}_{\tilde{x}(k)} \tag{9}$$

The modified state space representation given by Eq. (9) can be used as the input model for MPC algorithm.

3.2. Definition of the cost function

Typically, the objective function in MPC consists of the quadratic forms of the tracking error and the control input as given below:

$$J = \| Y(k+1) - Y_{ref}(k+1) \|_Q^2 + \| \Delta U(k) \|_R^2 \tag{10}$$

In Eq. (10), $Y_{ref}(k+1)$ denotes array of the reference outputs and the notation $\|x\|_R$ represents the weighted 2-norm. Also, $Y(k+1) = [\tilde{y}(k+1|k) \;\; \tilde{y}(k+2|k) \;\; \cdots \;\; \tilde{y}(k+N_p|k)]^T$ and $\Delta U(k) = [\Delta u(k|k) \;\; \Delta u(k+1|k) \;\; \cdots \;\; \Delta u(k+N_c-1|k)]^T$ denote the output and input increment vectors, respectively. For estimation of battery SoP, the objective function can be defined as follows:

$$J = \| Z(k+1) - Z_{ref}(k+1) \|_Q^2 + \| \Delta I(k) \|_R^2 \tag{11}$$

where $Z(k+1)$ represents the predicted cell SoCs along the prediction horizon N_p and $\Delta I(k)$ contains the battery current increments along the control horizon N_c. The output reference can be SoC of 100% for the charge case and 0% for the discharge case. Therefore, the control objective is to find the battery applied current sequence which drives the SoC to its reference value while ensuring the SOA for battery current and the terminal voltage.

3.3. Solution of the constrained optimization problem

Assuming $Q = I_{N_p}$ and $R = \gamma I_{N_c}$ in Eq. (11), the online optimization problem is as follows:

$$\min_{\Delta I(k)} J = (Z(k+1) - Z_{ref}(k+1))^T (Z(k+1) - Z_{ref}(k+1)) + \gamma (\Delta I(k))^T (\Delta I(k)) \tag{12}$$

subject to:

$$\begin{cases} \tilde{x}(k+1) = \tilde{A}\tilde{x}(k) + \tilde{B}\Delta i(k) \\ \tilde{y}_z(k) = \tilde{C}_z \tilde{x}(k) = z(k); \; \tilde{C}_z = [1 \;\; 0 \;\; 0] \\ i_{\min} \le i(k) \le i_{\max} \\ v_{\min} \le V_t(k) \le v_{\max} \end{cases} \tag{13}$$

where $v_{\min}$, $v_{\max}$ are the minimum and maximum allowable cell voltages and $i_{\min}$, $i_{\max}$ are the allowable charge and discharge currents, respectively. Note that the output $\tilde{y}_z(k)$ equals the first element of the state vector. In order to solve the above on-line optimization problem, we try to describe Eqs. (12) and (13) consistent with the well-known Quadratic Programming (QP) problem formulations which are of the

form described by Eq. (14).

$$J = \frac{1}{2}\Delta U^T G \Delta U + f^T \Delta U;\ s.\ t.\ A\Delta U \le b \tag{14}$$

The elements of the output vector $Z(k+1)$ can be calculated sequentially:

$$\begin{aligned}
z(k+1) &= \tilde{C}_z\tilde{x}(k+1) = \tilde{C}_z(\tilde{A}\tilde{x}(k) + \tilde{B}\Delta i(k)) = \tilde{C}_z\tilde{A}\tilde{x}(k) + \tilde{C}_z\tilde{B}\Delta i(k)\\
z(k+2) &= \tilde{C}_z\tilde{x}(k+2) = \tilde{C}_z(\tilde{A}\tilde{x}(k+1) + \tilde{B}\Delta i(k+1))\\
&= \tilde{C}_z\tilde{A}\tilde{x}(k+1) + \tilde{C}_z\tilde{B}\Delta i(k+1)\\
&= \tilde{C}_z\tilde{A}^2\tilde{x}(k) + \tilde{C}_z\tilde{A}\tilde{B}\Delta i(k) + \tilde{C}_z\tilde{B}\Delta i(k+1)\\
&\vdots\\
z(k+N_p) &= \tilde{C}_z\tilde{A}^{N_p}\tilde{x}(k) + \sum_{j=1}^{N_c}\tilde{C}_z\tilde{A}^{N_p-j}\tilde{B}\Delta i(k+j-1)
\end{aligned} \tag{15}$$

Eq. (15) can be written in the matrix form given by Eq. (16).

$$\underbrace{\begin{bmatrix} z(k+1)\\ z(k+2)\\ \vdots\\ z(k+N_p)\end{bmatrix}}_{Z(k+1)} = \underbrace{\begin{bmatrix} \tilde{C}_z\tilde{A}\\ \tilde{C}_z\tilde{A}^2\\ \vdots\\ \tilde{C}_z\tilde{A}^{N_p}\end{bmatrix}}_{P_z}\tilde{x}(k) + \underbrace{\begin{bmatrix} \tilde{C}_z\tilde{B} & 0 & \cdots & 0\\ \tilde{C}_z\tilde{A}\tilde{B} & \tilde{C}_z\tilde{B} & \cdots & 0\\ \vdots & \vdots & \vdots & \vdots\\ \tilde{C}_z\tilde{A}^{N_p-1}\tilde{B} & \tilde{C}_z\tilde{A}^{N_p-2}\tilde{B} & \cdots & \tilde{C}_z\tilde{A}^{N_p-N_c}\tilde{B}\end{bmatrix}}_{H_z}\Delta I(k) \tag{16}$$

Using Eq. (16), the objective function of Eq. (12) can be expanded as follows:

$$\begin{aligned}
J &= (P\tilde{x}(k) + H\Delta I(k) - Z_{ref}(k+1))^T(P\tilde{x}(k) + H\Delta I(k) - Z_{ref}(k+1))\\
&\quad + \gamma(\Delta I(k))^T(\Delta I(k))\\
&= 2(H\Delta I(k))^T(P\tilde{x}(k) - Z_{ref}(k+1)) + (H\Delta I(k))^T H\Delta I(k)\\
&\quad + \gamma(\Delta I(k))^T(\Delta I(k)) + Const.\\
&= 2(\Delta I(k))^T H^T(P\tilde{x}(k) - Z_{ref}(k+1)) + (\Delta I(k))^T(H^TH + \gamma I)(\Delta I(k))\\
&\quad + Const.\\
&= \underbrace{(2H^T(P\tilde{x}(k) - Z_{ref}(k+1)))^T}_{f}(\Delta I(k))\\
&\quad + \frac{1}{2}(\Delta I(k))^T\underbrace{(2H^TH + 2\gamma I)}_{G}(\Delta I(k)) + Const.\\
&= \frac{1}{2}(\Delta I(k))^T G(\Delta I(k)) + f^T\Delta I(k) + Const.
\end{aligned} \tag{17}$$

Therefore, the objective function is written in the form of QP problem. However, the constraints on battery current and terminal voltage should also be imposed as functions of ΔU. For battery current constraints we have:

$$i_{\min} \le i(k+j) \le i_{\max};\ j = 1,\ 2,\ \ldots,N_c \tag{18}$$

In terms of current increments we have:

$$\begin{aligned}
i(k+1) &= \Delta i(k) + i(k)\\
i(k+2) &= \Delta i(k) + \Delta i(k+1) + i(k)\\
&\vdots\\
i(k+N_c) &= \left(\sum_{j=0}^{N_c-1}\Delta i(k+j)\right) + i(k)
\end{aligned} \tag{19}$$

In the matrix form, Eq. (19) can be written as below:

$$\underbrace{\begin{bmatrix} i(k+1)\\ i(k+2)\\ \vdots\\ i(k+N_c)\end{bmatrix}}_{I(k+1)} = \underbrace{\begin{bmatrix} 1 & 0 & \cdots & 0\\ 1 & 1 & & 0\\ \vdots & \vdots & \vdots & \vdots\\ 1 & 1 & \cdots & 1\end{bmatrix}}_{D}\underbrace{\begin{bmatrix} \Delta i(k)\\ \Delta i(k+1)\\ \vdots\\ \Delta i(k+N_c-1)\end{bmatrix}}_{\Delta I(k)} + \underbrace{\begin{bmatrix} i(k)\\ i(k)\\ \vdots\\ i(k)\end{bmatrix}}_{\tilde{i}(k)} \tag{20}$$

Therefore, Eq. (20) can be reformulated as below:

$$\begin{bmatrix} D\\ -D\end{bmatrix}\Delta I(k) \le \begin{bmatrix} \tilde{i}_{\max} - \tilde{i}(k)\\ -(\tilde{i}_{\min} - \tilde{i}(k))\end{bmatrix} \tag{21}$$

where $\tilde{i}_{max}$ and $\tilde{i}_{min} \in \Re^{N_c}$ are vectors built from the elements $i_{\min}$ and $i_{\max}$, respectively. For the terminal voltage constraints we have:

$$v_{\min} \le V_t(k+j) \le v_{\max};\ j = 1,\ 2,\ \ldots,N_p \tag{22}$$

In order to write the above inequality as function of current increments, we go back to Eq. (9). Following the same procedure as presented for obtaining $Z(k+1)$ in Eqs. (15) and (16), we can write:

$$\underbrace{\begin{bmatrix} \tilde{y}_v(k+1)\\ \tilde{y}_v(k+2)\\ \vdots\\ \tilde{y}_v(k+N_p)\end{bmatrix}}_{\tilde{Y}_v(k+1)} = \underbrace{\begin{bmatrix} \tilde{C}_v\tilde{A}\\ \tilde{C}_v\tilde{A}^2\\ \vdots\\ \tilde{C}_v\tilde{A}^{N_p}\end{bmatrix}}_{P_v}\tilde{x}(k) + \underbrace{\begin{bmatrix} \tilde{C}_v\tilde{B} & 0 & \cdots & 0\\ \tilde{C}_v\tilde{A}\tilde{B} & \tilde{C}_v\tilde{B} & \cdots & 0\\ \vdots & \vdots & \vdots & \vdots\\ \tilde{C}_v\tilde{A}^{N_p-1}\tilde{B} & \tilde{C}_v\tilde{A}^{N_p-2}\tilde{B} & \cdots & \tilde{C}_v\tilde{A}^{N_p-N_c}\tilde{B}\end{bmatrix}}_{H_v}\Delta I(k) \tag{23}$$

Therefore, Eq. (22) can be represented as function of current increments as below:

$$\begin{bmatrix} H_v\\ -H_v\end{bmatrix}\Delta I(k) \le \begin{bmatrix} \tilde{v}_{\max} - \tilde{v}_{oc}(z(k)) - P_v\tilde{x}(k)\\ -(\tilde{v}_{\min} - \tilde{v}_{oc}(z(k)) - P_v\tilde{x}(k))\end{bmatrix} \tag{24}$$

where $\tilde{v}_{max}$, $\tilde{v}_{min}$, $\tilde{v}_{oc}(z(k)) \in \Re^{N_p}$ are vectors which are built from the elements $v_{\min}$, $v_{\max}$ and $V_{oc}(z(k))$, respectively. Combining the constraints on current and voltage, the following inequality constraint is obtained:

$$\underbrace{\begin{bmatrix} D\\ -D\\ H_v\\ -H_v\end{bmatrix}}_{A}\Delta I(k) \le \underbrace{\begin{bmatrix} \tilde{i}_{\max} - \tilde{i}(k)\\ -(\tilde{i}_{\min} - \tilde{i}(k))\\ \tilde{v}_{\max} - \tilde{v}_{oc}(z(k)) - P_v\tilde{x}(k)\\ -(\tilde{v}_{\min} - \tilde{v}_{oc}(z(k)) - P_v\tilde{x}(k))\end{bmatrix}}_{b} \tag{25}$$

The resulting QP problem of Eq. (17) subject to the inequality constraint of Eq. (25) can be solved using a standard solver such as the active set method to find the vector of current increments.

3.4. New cell SoP estimation

According to what developed in the previous sections, the new cell SoP for each of the charge and discharge cases can be predicted through the following steps:

- Step 1: The operating constraints for the applied $LiFePO_4$ cell, prediction and control horizons N_p and N_c and the weight parameter γ are chosen.
- Step 2: The matrices G, f, A and b of the QP problem are computed according to the new cell data obtained in the previous section.
- Step 3: The optimal current increments $\Delta I(k)$ is calculated at each time sample using a standard QP problem solver considering the output SoC references of 100% for the charge case and 0% for discharge.
- Step 4: Using the state space model of Eq. (9), the cell voltages along the prediction horizon are computed applying the optimal current increments $\Delta I(k)$ obtained in Step 3.
- Step 5: Multiplying the optimal current with the resulting cell voltage for each time sample along the prediction horizon, a vector of available power values is calculated. Then, the SoP for the new cell is computed using the following equations:

$$\begin{aligned}
SoP_{dis}^{MPC} &= \min(P_{dis}^1,\ P_{dis}^2,\ldots,P_{dis}^{N_p})\\
SoP_{chg}^{MPC} &= \max(P_{chg}^1,\ P_{chg}^2,\ldots,P_{chg}^{N_p})
\end{aligned} \tag{26}$$

The aforementioned MPC-based estimation of the SoP for the new cell is used as a basis for calculation of the SoP for an aged battery pack consisting of series-connected cells.

4. State of power estimation for series-connected cells

The new cell based SoP prediction developed in the previous section is used as the basis for estimation of the pack power capability. Assuming N_s to be the number of cells connected in series, the base estimate of pack SoP can be calculated as follows:

$$SoP_{dis}^{b} = N_s SoP_{dis}^{MPC}$$
$$SoP_{chg}^{b} = N_s SoP_{chg}^{MPC} \quad (27)$$

where SoP_{dis}^{MPC} and SoP_{chg}^{MPC} are defined by Eq. (26). We aim to propose a model-less control system to obtain the actual pack SoP through a closed-loop modification of the base SoP. The model-less control system establishes a closed-loop interaction with the high-level control unit, which is the VCU in this study. Since the same current passes through the series-connected cells, the terminal voltage of the cells reflects the differences in dynamic behavior of the cells. Therefore, the actual values of the current and cell voltages are used as the inputs of the model-less control system to compensate for the influence of aging state and SoC differences of the cells on the pack actual power capability. The pack actual SoP is limited by the weakest cell which is the cell that first reaches the SOA limits. Therefore, the actual SoP can be acquired through adaptation of the base SoP estimation to the operating conditions of the weakest cell. The following sections explain the details of the proposed model-less control system design.

4.1. Model-less control system design for base SoP modification

As inferred from Eq. (1), the differences in voltage response of the cells in a battery pack reflect different impedance parameters and open circuit voltage of the cells. In this paper, we concentrate on the ECM parameters change caused by only the cell SoC and SoH (as an indicator of the cell aging state). Therefore, the designed control system uses the actual current and terminal voltage of the cells to modify the base SoP in a closed-loop manner so that the SoC and SoH differences of the cells are compensated. The fuzzy logic controller is shown to be an appropriate candidate for control of nonlinear systems due to its easy implementation and high flexibility [49–51]. In the current research, a Fuzzy Logic Based Controller (FLBC) is designed to adapt the base SoP estimation to various aging state and SoC of the cells according to online data of the weakest cell in the pack.

In order to prevent the current and terminal voltage of the cells exceeding the SOA limits, the adaptation process should be started before reaching the limits. Accordingly, as depicted in Fig. 5 (a), three operating regions are defined which determine the operating modes of the FLBC. Region III indicates the unsafe operating region in which the battery should be prevented to enter. In this regard, the parameters i_{max}, i_{min}, v_{max} and v_{min} are the SOA limits which are usually reported by the manufacturer. Region I and Region II indicate the SOA for the battery and the parameters i_s^{dis}, i_s^{chg}, v_s^{dis} and v_s^{chg} indicate the secondary limits from which the adaptation process is started to prevent the battery entering Region III. Note that if the load varies such a way that the battery remains in Region II, no modification of the base SoP is required. Therefore, in addition to the operating region and the current/voltage values as the inputs of the controller, the instant rate of change for battery current/voltage is also considered as the controller input.

According to what explained above, the structure of the FLBC designed for base SoP modification is depicted in Fig. 5 (b). According to the SOA limits of current and voltage and each of the charge and discharge cases, separate FLBCs are defined where the normalized inputs for each fuzzy controller is defined by Eq. (28).

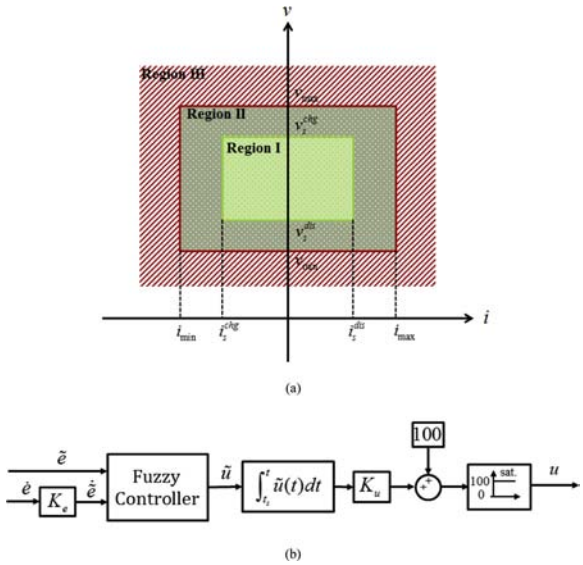

Fig. 5. (a) Operating regions of the battery, (b) structure of the FLBC.

$$\tilde{e} = \frac{e}{e^*},\ \dot{\tilde{e}} = K_e \dot{e} = K_e\left(\frac{de}{dt}\right)$$
$$(e,\ e^*) = \begin{cases} \text{Charge, current-based:}(i - i_{\min}^{chg},\ i_s^{chg} - i_{\min}^{chg}) \\ \text{Charge, voltage-based:}(v - v_{\max},\ v_s^{chg} - v_{\max}) \\ \text{Discharge, current-based:}(i - i_{\max}^{dis},\ i_s^{dis} - i_{\max}^{dis}) \\ \text{Discharge, voltage-based:}(v - v_{\min},\ v_s^{dis} - v_{\min}) \end{cases} \quad (28)$$

The parameters K_e and K_u are input and output scaling factors, respectively and t_s indicates the time at which the battery reaches the secondary limit. The output u determines the percentage of the base SoP which should be applied to limit the battery within its SOA. A 3-D view of the implemented fuzzy controller is depicted in Fig. 6, which explains the operating modes of the fuzzy controller. Also, the membership functions of the input/output variables are illustrated in Fig. 7. When the output u is 100%, no modification is performed on the base SoP. The output decreases from 100 if $\tilde{e}$ is PB (i.e. battery exceeds the secondary limit) and $\dot{\tilde{e}}$ is negative. Starting the modification process before reaching the SOA limits not only prevents the battery exceeding its SOA limits using the closed-loop interaction with the VCU, but also it can avoid rapid reduction of battery power in situations where the power request from the battery is temporarily high like during vehicle acceleration or regenerative braking.

The scaling factors K_e and K_u are obtained by trial and error and listed in Table 1. As mentioned, for each side of the safe operating region shown in Fig. 5 (a), a separate controller with the same structure as given by Fig. 5 (b) is developed. Therefore, the final output for the FLBC, named "charge/discharge correction coefficient", can be acquired by Eq. (29). The subscripts "*i*" and "*v*" indicate the current-based versus voltage-based modifications. The normalized correction coefficients are then multiplied by the obtained base SoP for each of the charge and discharge cases.

$$\bar{u}^{dis} = 0.01 \times \min(u_i^{dis},\ u_v^{dis})$$
$$\bar{u}^{chg} = 0.01 \times \min(u_i^{chg},\ u_v^{chg}) \quad (29)$$

4.2. Power capability estimation using hybrid MPC and FLBC

As mentioned before, the base SoP estimation should be modified

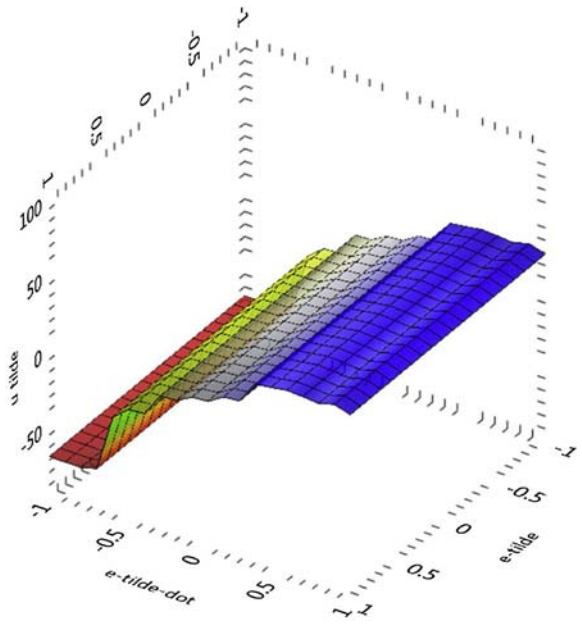

Fig. 6. 3-D view of the implemented fuzzy controller.

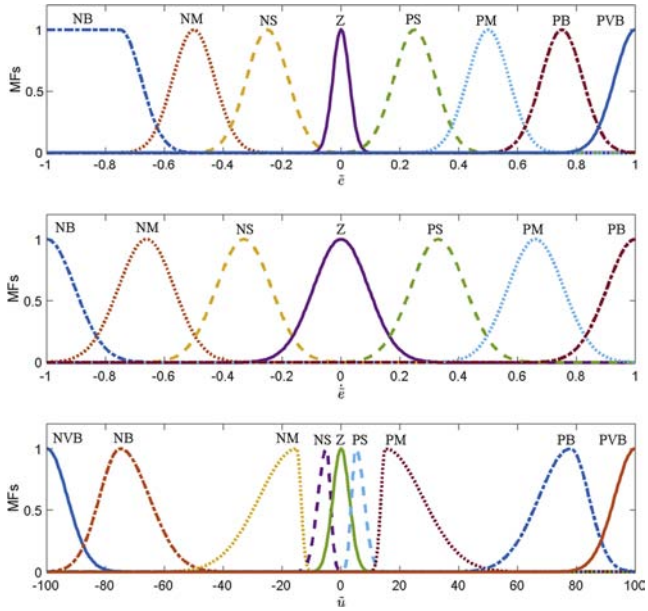

Fig. 7. Fuzzy controller membership functions.

Table 1
Values of the scaling factors.

Type of FLBC	Current-based		Voltage-based	
Scaling factor	K_e	K_u	K_e	K_u
Value	0.003	1.7	1	1.7

according to actual current and cell voltage values of the cell that first reaches the SOA limits. Fig. 8 (a) and Fig. 8 (b) illustrate the process of the pack actual SoP estimation for the charge and discharge cases, respectively. As shown, the MPC algorithm is applied for base SoP estimation using new cell data following the steps given in section 3.4. In the meanwhile, the SoC for a single new cell is the only state which is required to be co-estimated with the base SoP using Eq. (4). The current and maximum/minimum cell voltages are used as the inputs of the FLBC to obtain the percentage of the base SoP which should be applied to prevent the battery violating the SOA limits. As a result, the FLBC adapts the base SoP estimations to the current SoC and SoH states of the cells.

Referring to the definition of battery SoP, the maximum available battery power is achieved when the battery operates on the boundary of its SOA. As mentioned before, the FLBC prevents the actual current or cell voltages violating the allowable limits using a closed-loop interaction with VCU. In this case, battery operation on the SOA limits of current or voltage (depending whether the current or voltage acts as the power limiting factor) will be continued while the maximum available power is requested from the battery. This may occur, for example, during the acceleration or regenerative braking in which the requested power from the battery is high for a short time. The correspondence between the battery available power with its operation on the current or voltage SOA limits is used as a basis for modification of the SoP estimates. In this regard, in addition to transient modifications, if the time duration of battery operation on the SOA limits is equal to or more than the time window ΔT, the correction coefficient at the end of the time window determines the permanent modification which should be applied on the base SoP to obtain the pack actual power capability. Obviously, this type of modification will also be updated with the change of battery states when the same condition occurs.

5. Verification and discussion

The SoP estimation is commonly verified using constant current or constant voltage pulses [23]. This is due to the fact that the real available power of the battery for the upcoming time window in not known. Accordingly, the SoP estimation is accurate if one of the following is achieved:

1) One of the cell voltages *is equal to* or *hits* the SOA limits during the pulse (i.e. v_{min} or v_{max}) while the current is within its predefined allowable region (i.e. $i_{min} < i < i_{max}$).
2) The current *is equal to* or *hits* the SOA limits during the pulse (i.e. i_{min} or i_{max}) while the cell voltages are all within their predefined allowable region (i.e. $v_{min} < v < v_{max}$).

The true value of battery available power corresponds with the current or voltage value reaching exactly its allowable limits according to one of the above conditions. Accordingly, the relative estimation error can be defined as given by Eq. (30), which is similar to what proposed by Waag et al. [23].

$$RE(\%) = 100 \times \frac{\Delta P}{P} \approx 100 \times \left| \frac{v_k - v_{lim}}{v_{lim}} \right| or 100 \times \left| \frac{i_k - i_{lim}}{i_{lim}} \right| \quad (30)$$

The results are presented in two sections; First, the SoP is estimated using MPC algorithm for a single new cell and the results are compared with the previous studies. Then, the proposed hybrid MPC and FLBC method is evaluated in a feed-forward simulation model for a series hybrid electric city bus during driving cycle and the SoP estimations are verified for series-connected cells with different initial SoC and SoH values.

5.1. MPC-based SoP estimation results for new cell

In this section, the SoP estimation results for a single new cell are presented. Relevant MPC algorithm parameters are listed in Table 2. The estimations at three different SoCs of 30, 60 and 90% and time windows of one, five and ten seconds are given in Table 3. The simulation time step is chosen to be one millisecond. Also, for prediction windows of one, five and ten seconds, the SoP estimation time steps are assumed to be 0.1, 1, 1 s, respectively, which leads to prediction horizons of 10, 5 and 10, respectively. The results are compared with those developed by Sun et al. [27] in which the cell SoP is estimated assuming

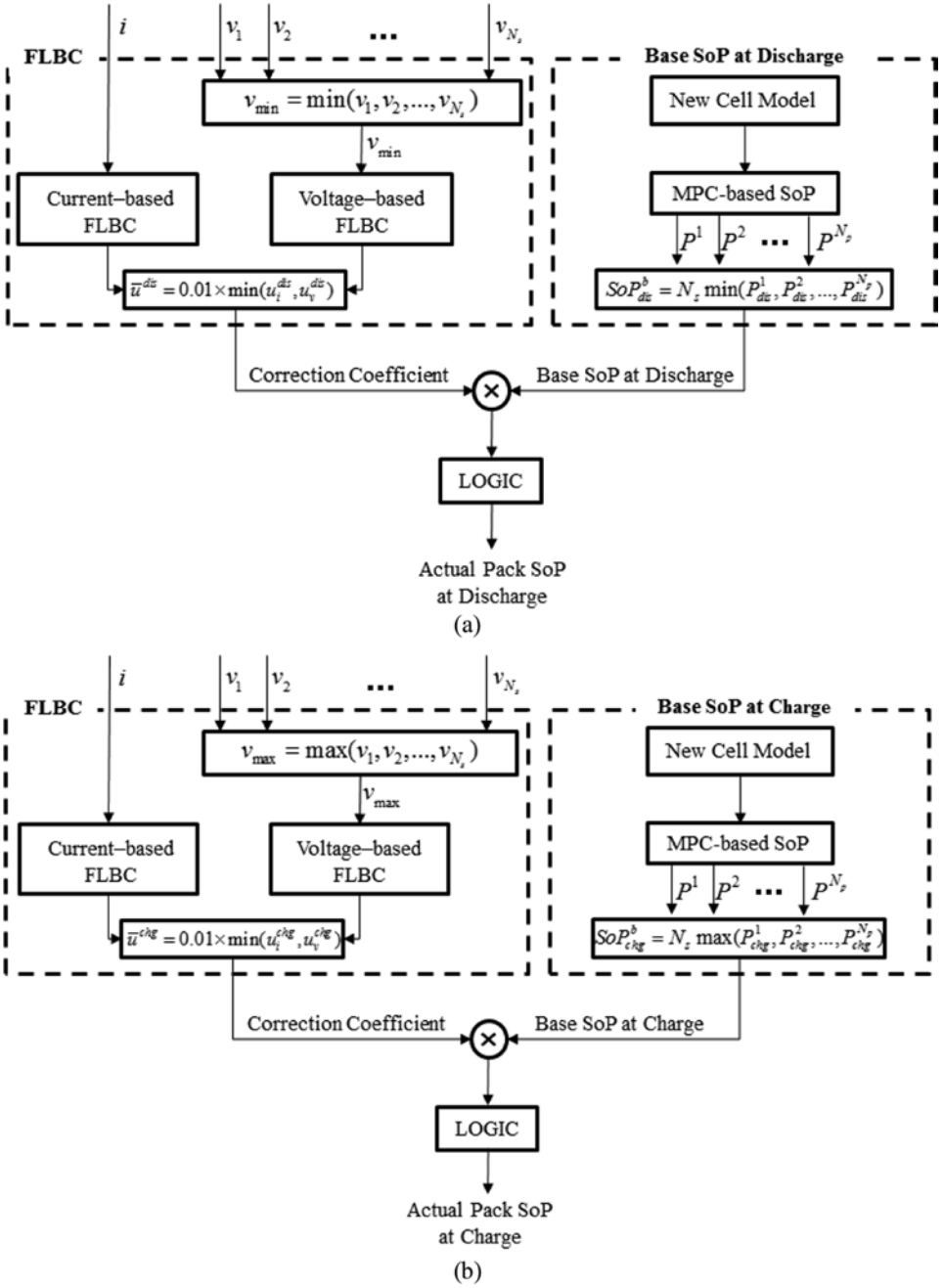

Fig. 8. The actual SoP estimation for the battery pack using hybrid MPC and FLBC, (a) discharge SoP, (b) charge SoP.

Table 2
Relevant MPC parameters for SoP estimation.

Parameter	N_p	N_c	γ	z_{ref}^{chg}	z_{ref}^{dis}	i_{max}	i_{min}	v_{max}	v_{min}
Value	5,10	1	10^{-7}	1	0	150 A	−30 A	3.65 V	2.1 V

a constant-current mode for the entire prediction horizon. In Ref. [27], the maximum (minimum) *constant* discharge (charge) current which leads to the voltage reaching its minimum (maximum) limit at the end of the time window is calculated. Then, the battery available power for the upcoming time window is computed through multiplication of the obtained current with its resulting voltage at the end of the prediction horizon, i.e. at time $t+\Delta T$. In order to be similar with Ref. [27], the control horizon is assumed to be one for all cases so that the constant-current mode is provided.

In order to compare and verify the estimation results, the estimated available power for each method is applied to the battery for ΔT seconds and the relative error for each case is calculated. As shown in Figs. 9 and 10, the average relative errors for MPC-based estimation method are 1.81% and 0.27% for the discharge and charge cases, respectively, while these values for the estimation method of Ref. [27] are 3.59% and 0.79%, respectively.

For a detailed evaluation, the change in battery current, voltage and SoP estimates during the prediction time window are represented for two sample cases. Fig. 11(a) to (c) show the verification test results for the case in which the prediction time window and the initial SoC are one second and 30%, respectively. In this test, as depicted in Fig. 11 (a), the estimated available power at charge and discharge cases are applied to the battery constantly for one second. The upcoming estimates of SoP during the time window are also depicted in Fig. 11 (a) where the applied power is equal to the initial estimate of available power, as

Table 3
MPC-based SoP estimation results compared with Sun et al. method.

SoC (%)	State	*SoP (W), MPC method*			*SoP (W), Sun et al. method*		
		$\Delta T = 1$ sec	$\Delta T = 5$ sec	$\Delta T = 10$ sec	$\Delta T = 1$ sec	$\Delta T = 5$ sec	$\Delta T = 10$ sec
30	Charge	−105.631	−105.631	−94.0581	−106.326	−108.757	−94.6842
	Discharge	312.61	256.73	204.315	310.358	243.514	196.955
60	Charge	−105.968	−105.968	−104.423	−106.432	−108.142	−104.357
	Discharge	290.202	250.039	208.526	288.657	239.946	202.366
90	Charge	−107.622	−95.8203	−72.7666	−108.403	−92.2741	−72.6957
	Discharge	304.96	238.589	187.11	302.025	224.693	180.644

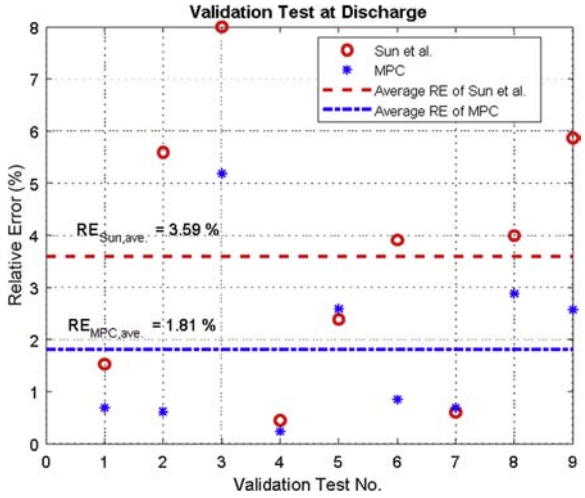

Fig. 9. MPC-based relative estimation error at discharge compared with Sun et al. method.

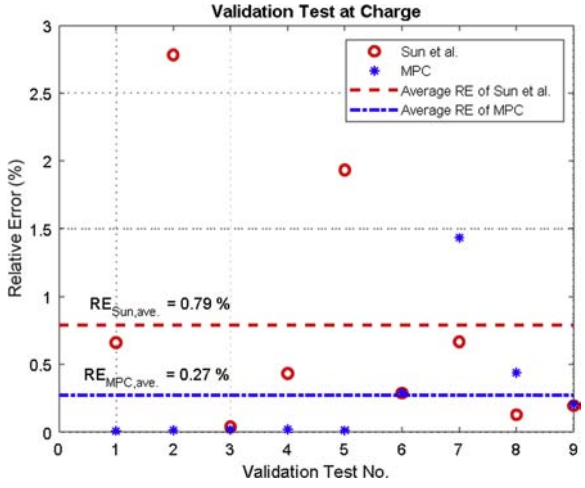

Fig. 10. MPC-based relative estimation error at charge compared with Sun et al. method.

expected. Fig. 11 (b) and (c) show the change of battery current and voltage during the time window, respectively. For the charge case, as can be concluded, the battery current is the limiting factor for obtaining the available power. Therefore, the deviation between the current and its minimum allowable value (which equals -30 A) is an indicator of SoP estimation accuracy. As can be seen in Figs. 11 (b) and Fig. 10 (validation test number one), the relative error in this case is near zero for the MPC-based estimation while the method of Ref. [27] results in the relative error of about 0.7%. For the discharge case, the limiting factor is the voltage and therefore, the deviation between the cell voltage and the minimum allowable value of 2.1 V at the end of the time window indicates the relative accuracy of SoP estimation which is compared in Fig. 9 (validation test number one).

For the case in which the prediction time window and the initial SoC are ten seconds and 90%, respectively, the results are shown in Fig. 11 (d) to (f). In this case, the cell voltage acts as the limiting factor for the available power achievement in both of the charge and discharge conditions. As depicted in Fig. 11 (f) and Fig. 10 (validation test number nine), the relative errors for both methods are nearly the same for the discharge case. However, for the charge case, the relative estimation errors for the MPC-based method and Sun et al. method are 2.6% and 5.9%, respectively.

According to what presented in this section, it can be concluded that using MPC algorithm, the accuracy of SoP estimations is improved, thus providing a better safe performance of the battery in sense of the ability to deliver or receive power.

5.2. Series-connected cells SoP estimation results

In this section, the series HEV simulation model results are presented [52]. But first, in order to evaluate the computational cost of the present method, the total computation time for the SoP estimation method in different test cycles are compared with those presented by Jiang et al. [38]. The estimation methods are executed on a PC with 2.4 GHz CPU and 4 GB RAM. As given in Table 4, the proposed technique reduces the computational cost while achieving accurate estimations of battery pack power capability, as will be demonstrated in the following. This is due to the fact that in Ref. [38] the ECM parameters of all the cells should be identified on-line in order to consider their different aging states. But in the present methodology, only the new cell ECM parameters are utilized which are identified off-line.

As explained in section 4, the model-less FLBC uses the actual current and cell voltages to modify the base SoP estimates through a closed-loop interaction with the VCU. Accordingly, the pack-level SoP estimates are evaluated using a feed-forward simulation model for a series hybrid electric city bus which is investigated in Tehran heavy duty vehicle driving cycle [52]. Without loss of generality, the results are obtained assuming that each battery pack is made up of four series-connected $LiFePO_4$ cells with the initial states given in Table 5. The battery pack consists of the new and aged cells with different initial SoC values.

For verification, the ECM for a sample aged cell is extracted using the experimental setup in just the same way as the new cell. The capacity of the sample aged cell is obtained to be 9.84 Ah using the procedure explained in section 2.2. The actual cell voltage for the aged cell sample is then obtained from the ECM and used as inputs of the SoP estimation method. The time step for estimation of the SoP is assumed to be 250 ms and the prediction and control horizons are considered to be 4 and 2, respectively, which means that the estimation is performed for the prediction time window of one second.

Fig. 12 shows the results applying the hybrid MPC and FLBC for battery pack SoP estimation. As shown in Fig. 12 (a) and (b), during the first half of the cycle, the battery operates within the safe operating region and therefore, no modification is performed on the base SoP

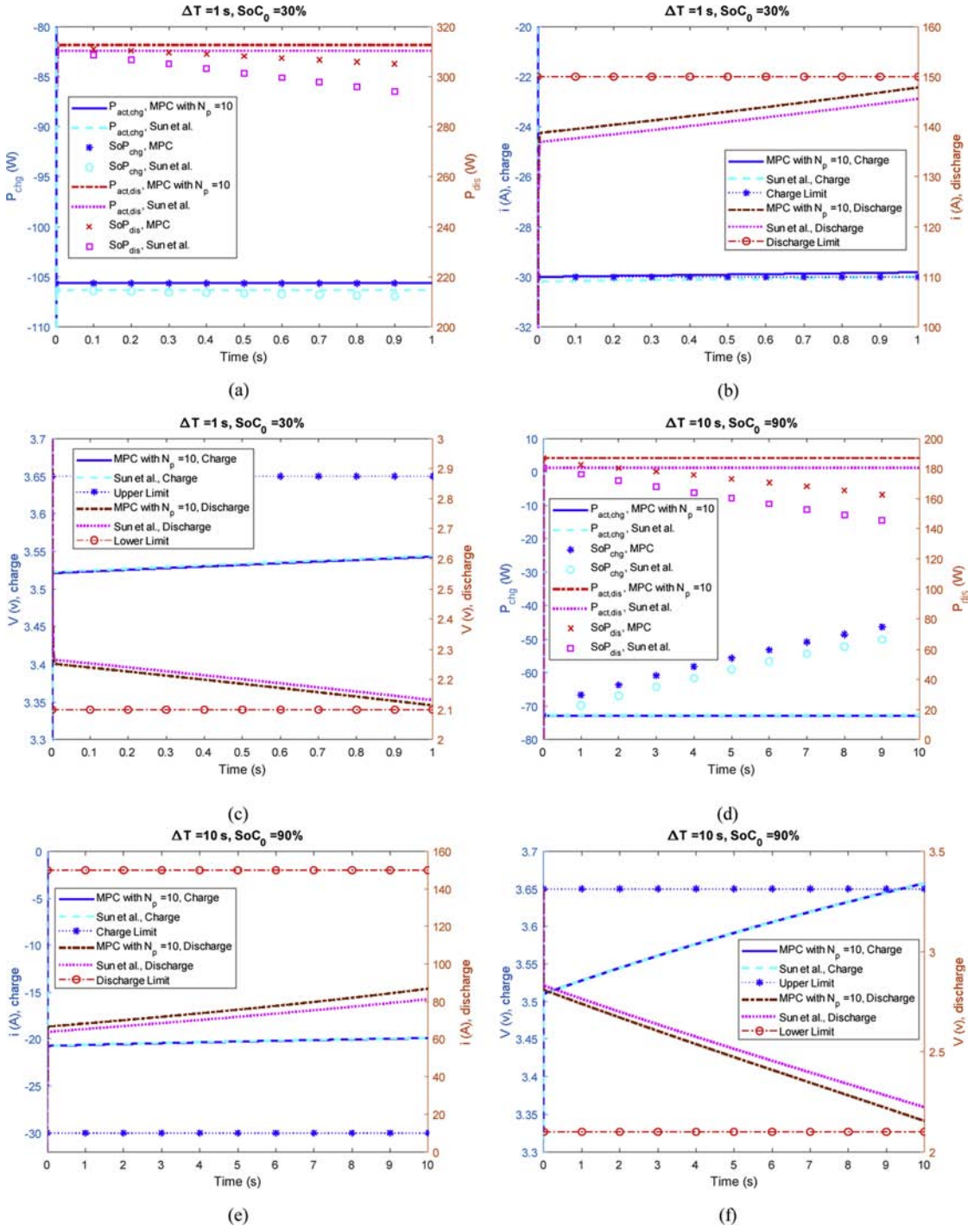

Fig. 11. Verification tests for MPC-based estimation versus Sun et al. method for two sample cases of $\Delta T = 1$ s, $SoC_0 = 30\%$ and $\Delta T = 10$ s, $SoC_0 = 90\%$, (a), (d) maximum/minimum power, (b), (e) current, (c), (f) voltage.

Table 4
Computational cost of the present method compared with Ref. [38].

Test Cycles	Computation Time (seconds)		Time Reduced (%)
	Ref. [38]	Present Method	
NEDC	1.28	0.95	25.8
FTP75	2.66	1.83	31.2

estimation. For the discharge case, the under-voltage limit reaches earlier than the discharge current limit and the power capability is consequently limited by the cell voltages. In this case, modification of the base SoP is started at around the 955th second of the cycle where at least one cell is reaching the voltage limit. This time interval of the cycle is magnified in Fig. 13 (a) to provide a close observation of the results. The weakest cell at this time is Cell 1 which first reaches the voltage limit. At this time, the base SoP is modified using the discharge correction coefficient which decreases from 100% (Fig. 12 (d)) to compensate for the aging state and SoC differences between the cells.

Table 5
Initial state of the cells for verification test.

Cell number	Cell 1			Cell 2			Cell 3			Cell 4		
State	SoC	SoH	Capacity (Ah)	SoC	SoH	Capacity (Ah)	SoC	SoH	Capacity (Ah)	SoC	SoH	Capacity (Ah)
Value	58%	Aged	9.84	62%	Aged	9.84	59%	New	10.58	56%	New	10.58

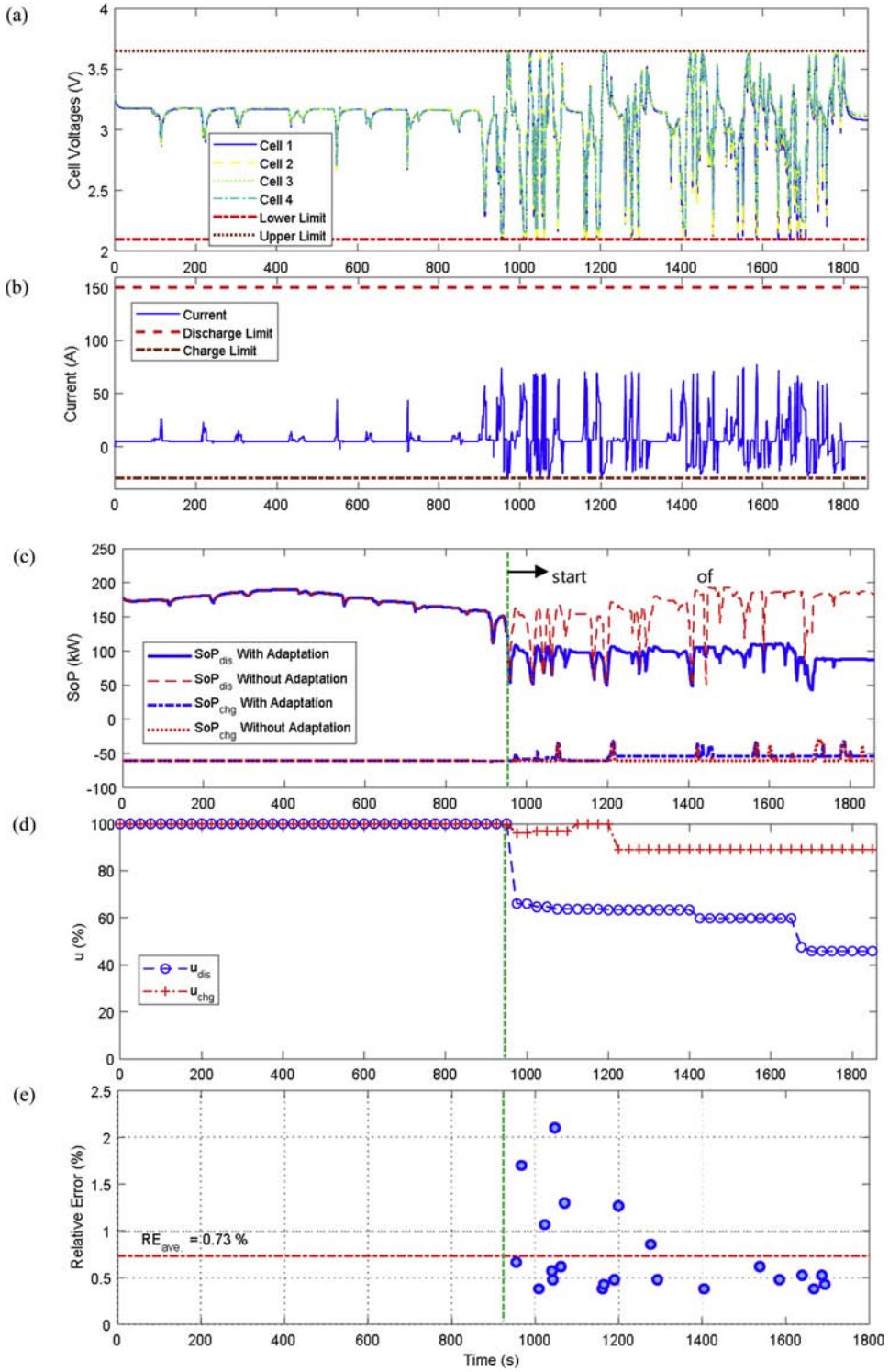

Fig. 12. Hybrid MPC and FLBC results in Tehran driving cycle, (a) cell voltages, (b) current, (c) SoP estimations, (d) correction coefficients, (e) relative estimation error.

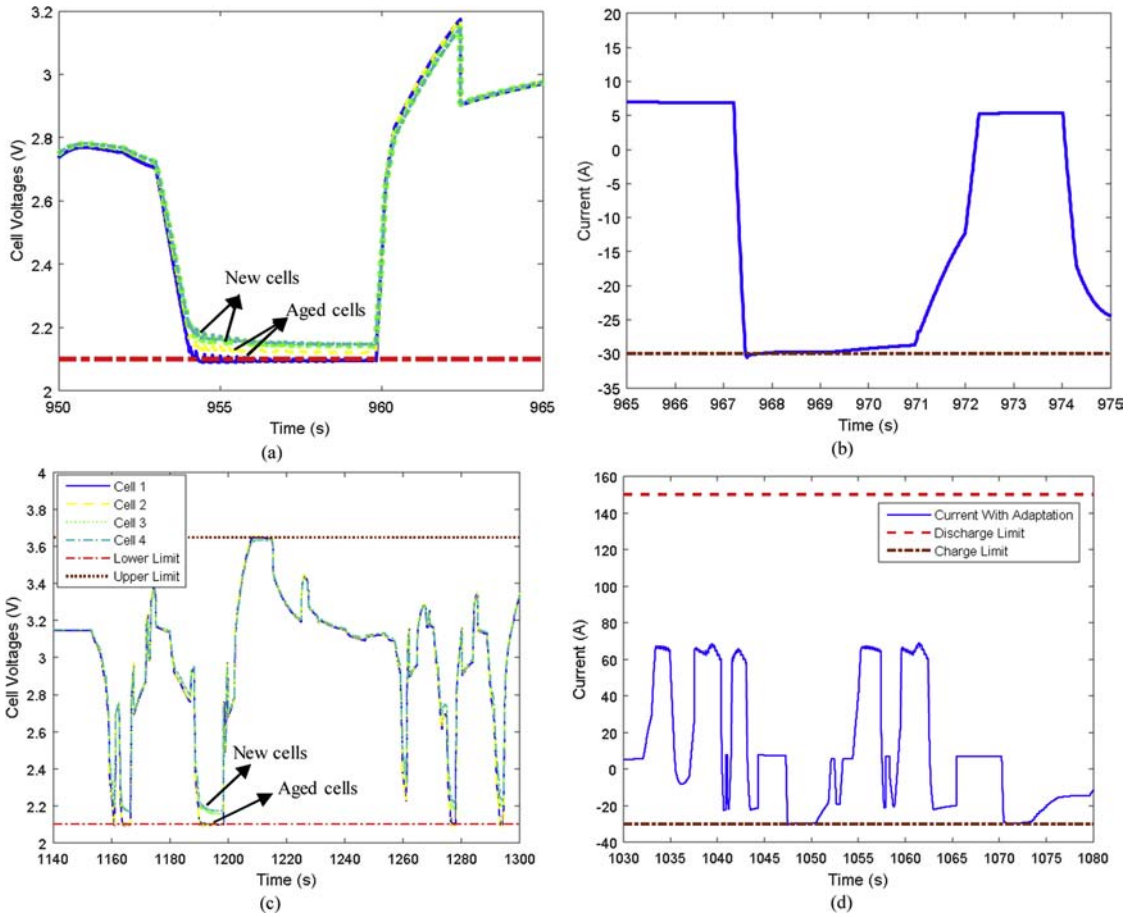

Fig. 13. (a) Start of discharge SoP modification, (b) start of charge SoP modification, (c), (d) magnified intervals of the cycle.

The power capability on charging is limited by the current since the current limit (i.e. i_{min} = -30 A) reaches sooner than the voltage limit (i.e. v_{max} = 3.65 V). The first modification on the charge base SoP is applied around the 968th second of the cycle as depicted in Fig. 12 (b). At this time, the charge correction coefficient decreases from 100% (Fig. 12 (d)) to correct the base SoP estimation. The effect of the modification process on battery current can be seen in Fig. 13 in a magnified view where the charge current is controlled not to violate its allowable region.

In Fig. 12 (c), the estimated SoP for the pack is compared with the case in which no adaptation to the aging state and SoC variations among the cells is considered. By starting the adaptation process, the base SoP estimate is limited to prevent the weakest cell violating the allowable current or voltage boundaries.

Fig. 12 (e) represents the relative estimation errors for the voltage or current pulses during the cycle which are obtained from Eq. (30). As mentioned previously, the definition of the relative estimation error differs for the current and voltage pulses depending whether the current or voltage acts as the limiting factor for the pack power capability. As can be seen, the average relative error for the whole cycle is about 0.73% and its maximum value is about 1.7%.

The results indicate that utilizing only the ECM parameters of the new cell, which are identified off-line, the SoP is estimated accurately for series-connected cells with concurrent SoC and SoH differences. Moreover, the safe current and voltage operating regions for all the cells are guaranteed in HEV which again proves the effectiveness of the present method.

6. Conclusion

In the present study, a new approach is proposed to estimate the SoP for a Lithium-ion battery pack considering the concurrent SoH and SoC variations of the cells. A MPC-based algorithm is first employed to obtain a base estimation of SoP for an assumed balanced new pack. Accordingly, at nine different cases, the estimations are verified and compared with those obtained by the most common SoP estimation method and the results confirm the higher accuracy of MPC-based estimations. At the second stage, a fuzzy logic based control system is designed to modify the MPC-based estimations compensating for the inconsistencies present in SoH and SoC values of the cells. In this regard, the actual current and cell voltages are used in a closed-loop framework, thereby eliminating the need for on-line co-estimation of SoH and SoC values for the cells together with the SoP estimation to consider the cell-to-cell inconsistencies. Experiment and simulation results prove the promising performance of the proposed method towards accurate estimation of the power capability and guaranteed safe operation of the battery pack. The future work will focus on the inclusion of battery temperature variation and hardware-in-the-loop simulation of the proposed SoP estimation technique.

Acknowledgment

This work has benefitted greatly from the supports of Vehicle, Fuel and Environment Research Institute (VFERI), University of Tehran.

References

[1] R. Wegmann, V. Döge, D.U. Sauer, Assessing the potential of an electric vehicle hybrid battery system comprising solid-state lithium metal polymer high energy and lithium-ion high power batteries, J. Energy Storage 18 (2018) 175–184.
[2] Q. Kellner, E. Hosseinzadeh, G. Chouchelamane, W.D. Widanage, J. Marco, Battery cycle life test development for high-performance electric vehicle applications, J. Energy Storage 15 (2018) 228–244.
[3] J. Jaguemont, L. Boulon, Y. Dubé, A comprehensive review of lithium-ion batteries used in hybrid and electric vehicles at cold temperatures, Appl. Energy 164 (2016) 99–114.
[4] F.J. Soares, et al., The STABALID project: risk analysis of stationary Li-ion batteries for power system applications, Reliab. Eng. Syst. Saf. 140 (2015) 142–175.
[5] H. Dreger, W. Haselrieder, A. Kwade, Influence of dispersing by extrusion and calendering on the performance of lithium-ion battery electrodes, J. Energy Storage 21 (2019) 231–240.
[6] X. Li, L. Zhang, Z. Wang, P. Dong, Remaining useful life prediction for lithium-ion batteries based on a hybrid model combining the long short-term memory and Elman neural networks, J. Energy Storage 21 (2019) 510–518.
[7] C. Campestrini, M.F. Horsche, I. Zilberman, T. Heil, T. Zimmermann, A. Jossen, Validation and benchmark methods for battery management system functionalities: state of charge estimation algorithms, J. Energy Storage 7 (2016) 38–51.
[8] K. Liu, K. Li, Q. Peng, C. Zhang, A brief review on key technologies in the battery management system of electric vehicles, Front. Mech. Eng. (April) (2018).
[9] A. Abdollahi, et al., Optimal charging for general equivalent electrical battery model, and battery life management, J. Energy Storage 9 (2017) 47–58.
[10] X. Hu, N. Murgovski, L. Johannesson, B. Egardt, Energy efficiency analysis of a series plug-in hybrid electric bus with different energy management strategies and battery sizes, Appl. Energy 111 (2013) 1001–1009.
[11] W. Waag, C. Fleischer, D.U. Sauer, Critical review of the methods for monitoring of lithium-ion batteries in electric and hybrid vehicles, J. Power Sources 258 (2014) 321–339.
[12] M. Masih-Tehrani, M. Dahmardeh, A Novel Power Distribution System Employing State of Available Power Estimation for a Hybrid Energy Storage System, IEEE Trans. Ind. Electron. 65 (August 8) (2018) 6676–6685.
[13] C. Fleischer, W. Waag, H.-M. Heyn, D.U. Sauer, On-line adaptive battery impedance parameter and state estimation considering physical principles in reduced order equivalent circuit battery models part 2. Parameter and state estimation, J. Power Sources 262 (September) (2014) 457–482.
[14] A. Farmann, D. Uwe, A comprehensive review of on-board State-of-Available-Power prediction techniques for lithium-ion batteries in electric vehicles, J. Power Sources 329 (2016) 123–137.
[15] X. Zhang, Y. Wang, J. Wu, Z. Chen, A novel method for lithium-ion battery state of energy and state of power estimation based on multi-time-scale filter, Appl. Energy 216 (September) (2017) 442–451 2018.
[16] C. Fleischer, W. Waag, Z. Bai, D.U. Sauer, Adaptive on-line state-of-available-power prediction of lithium-ion batteries, J. Power Electron. 13 (4) (2013) 516–527.
[17] Y. Wang, R. Pan, C. Liu, Z. Chen, Q. Ling, Power capability evaluation for lithium iron phosphate batteries based on multi-parameter constraints estimation, J. Power Sources 374 (January) (2018) 12–23.
[18] S. Wang, M. Verbrugge, J.S. Wang, P. Liu, Power prediction from a battery state estimator that incorporates diffusion resistance, J. Power Sources 214 (2012) 399–406.
[19] R. Xiong, F. Sun, H. He, T. Duy, A data-driven adaptive state of charge and power capability joint estimator of lithium-ion polymer battery used in electric vehicles, Energy 63 (2013) 295–308.
[20] R. Xiong, H. He, F. Sun, K. Zhao, Online estimation of peak power capability of Li-Ion batteries in electric vehicles by a hardware-in-the-loop approach, Energies 5 (May 5) (2012) 1455–1469.
[21] W. Waag, C. Fleischer, D.U. Sauer, On-line estimation of lithium-ion battery impedance parameters using a novel varied-parameters approach, J. Power Sources 237 (2013) 260–269.
[22] C. Fleischer, W. Waag, H.M. Heyn, D.U. Sauer, On-line adaptive battery impedance parameter and state estimation considering physical principles in reduced order equivalent circuit battery models part 2. Parameter and state estimation, J. Power Sources 262 (2014) 457–482.
[23] W. Waag, C. Fleischer, D. Uwe, Adaptive on-line prediction of the available power of lithium-ion batteries, J. Power Sources 242 (2013) 548–559.
[24] C. Burgos-Mellado, M.E. Orchard, M. Kazerani, R. Cardenas, D. Saez, Particle-filtering-based estimation of maximum available power state in Lithium-Ion batteries, Appl. Energy 161 (January) (2016) 349–363.
[25] Z. Wei, S. Meng, B. Xiong, D. Ji, K.J. Tseng, Enhanced online model identification and state of charge estimation for lithium-ion battery with a FBCRLS based observer, Appl. Energy 181 (2016) 332–341.
[26] Z. Wei, J. Zhao, D. Ji, K.J. Tseng, A multi-timescale estimator for battery state of charge and capacity dual estimation based on an online identified model, Appl. Energy 204 (2017) 1264–1274.
[27] F. Sun, R. Xiong, H. He, Estimation of state-of-charge and state-of-power capability of lithium-ion battery considering varying health conditions, J. Power Sources 259 (2014) 166–176.
[28] Z. Wei, J. Zhao, R. Xiong, G. Dong, J. Pou, K.J. Tseng, Online estimation of power capacity with noise effect attenuation for lithium-ion battery, IEEE Trans. Ind. Electron. 66 (7) (2019) 5724–5735.
[29] M.F. Samadi, M. Saif, Nonlinear model predictive control for cell balancing in Li-ion battery packs, 2014 American Control Conference, (2014), pp. 2924–2929.
[30] G. Kujundžić, Š. Ileš, J. Matuško, M. Vašak, Optimal charging of valve-regulated lead-acid batteries based on model predictive control, Appl. Energy 187 (February) (2017) 189–202.
[31] M. Torchio, L. Magni, R.D. Braatz, D.M. Raimondo, Design of piecewise affine and linear time-varying model predictive control strategies for advanced battery management systems, J. Electrochem. Soc. 164 (4) (2017) A949–A959.
[32] M.A. Xavier, M.S. Trimboli, Lithium-ion battery cell-level control using constrained model predictive control and equivalent circuit models, J. Power Sources 285 (July) (2015) 374–384.
[33] M.A. Xavier, Efficient Strategies for Predictive Cell-level Control of Lithium-Ion Batteries, PhD. thesis Univ. Color. Color. Springs, 2019.
[34] K. Liu, K. Li, C. Zhang, Constrained generalized predictive control of battery charging process based on a coupled thermoelectric model, J. Power Sources 347 (2017) 145–158.
[35] C. Fleischer, W. Waag, Z. Bai, D.U. Sauer, On-line self-learning time forward voltage prognosis for lithium-ion batteries using adaptive neuro-fuzzy inference system, J. Power Sources 243 (2013) 728–749.
[36] Z. Jin, Z. Zhang, T. Aliyev, A. Rick, B. Sisk, Estimating the power limit of a Lithium battery pack by considering cell variability, SAE Technical Paper (2015).
[37] G. Dong, Z. Chen, J. Wei, A method for peak power prediction of series-connected lithium-ion battery pack using extended Kalman filter, Int. J. Mech. Eng. Robot. Res. 6 (2) (2017) 134–139.
[38] B. Jiang, H. Dai, X. Wei, L. Zhu, Z. Sun, Online reliable peak Charge/Discharge power estimation of series-connected lithium-ion battery packs, Energies 10 (3) (2017) 390.
[39] Z. Jin, Z. Zhang, P. Wyatt, Integrating feedback control algorithms with the lithium-ion battery model to improve the robustness of real time power limit estimation, SAE Techn. Pap. (2017).
[40] S. Nejad, D.T. Gladwin, D.A. Stone, A systematic review of lumped-parameter equivalent circuit models for real-time estimation of lithium-ion battery states, J. Power Sources 316 (2016) 183–196.
[41] T. Wik, B. Fridholm, H. Kuusisto, Implementation and robustness of an analytically based battery state of power, J. Power Sources 287 (2015) 448–457.
[42] S. Ag, Softing CAN Layer2 Manual Software Description, no. February (2009).
[43] G.L. Plett, Battery Management Systems: Volume I, Battery Modelling, Artech House, 2015.
[44] G. Dong, J. Wei, Z. Chen, Kalman filter for onboard state of charge estimation and peak power capability analysis of lithium-ion batteries, J. Power Sources 328 (2016) 615–626.
[45] E.F. Camacho, C.B. Alba, Model Predictive Control, Springer Science & Business Media, 2013.
[46] L. Wang, Model Predictive Control System Design and Implementation Using MATLAB, (2009).
[47] M.A. Xavier, Lithium-ion battery cell management: A model predictive control approach, Master's thesis Univ. Color. Color. Springs, 2019.
[48] A.W. Ordys, A.W. Pike, State space generalized predictive control incorporating direct through terms, Proc. 37th IEEE Conf. Decis. Control (Cat. No.98CH36171) 4 (December) (1998) 4740–4741.
[49] E. Mohammadi, M. Montazeri-Gh, P. Khalaf, Metaheuristic design and optimization of fuzzy-based gas turbine engine fuel controller using hybrid Invasive weed optimization/Particle swarm optimization algorithm, J. Eng. Gas Turbines Power 136 (November 3) (2013) p. 031601.
[50] E. Mohammadi, M. Montazeri-Gh, A fuzzy-based gas turbine fault detection and identification system for full and part-load performance deterioration, Aerosp. Sci. Technol. 46 (October) (2015) 82–93.
[51] L.-X. Wang, A Course in Fuzzy Systems, Prentice-Hall press, USA, 1999.
[52] M. Montazeri, M. Arefian, Development of the first driving cycle for Tehran City buses using Markov Chain and transition analysis, First Conference of Environmental Engineering, (2007).